

# LIMNOLOGY and OCEANOGRAPHY: METHODS



Limnol. Oceanogr.: Methods 22, 2024, 321–332 © 2024 Association for the Sciences of Limnology and Oceanography. doi: 10.1002/jom3.10609

# Development of a fast-response system with integrated calibration for high-resolution mapping of dissolved methane concentration in surface waters

Jesse T. Dugan ,\* Thomas Weber, John D. Kessler

Department of Earth and Environmental Sciences, University of Rochester, Rochester, New York, USA

### **Abstract**

Dissolved gas concentrations in surface waters can have sharp gradients across marine and freshwater environments, which often prove challenging to capture with analytical measurement. Collecting discrete samples for laboratory analysis provides accurate results, but suffers from poor spatial resolution. To overcome this limitation, water equilibrators and gas membrane contactors (GMCs) have been used for the automated underway measurement of dissolved gas concentrations in surface water. However, while water equilibrators can provide continuous measurements, their analytical response times to changes in surface water concentration can be slow, lasting tens of minutes. This leads to spatial imprecisions in the dissolved gas concentration data. Conversely, while GMCs have proven to have much faster analytical response times, often lasting only a few minutes or less, they suffer from poor accuracy and thus require routine calibration. Here we present an analytical system for the high accuracy and high precision spatial mapping of dissolved methane concentration in surface waters. The system integrates a GMC with a cavity ringdown spectrometer for fast analytical response times, with a calibration method involving two Weiss-style equilibrators and discrete measurements in vials. Data from both the GMC and equilibrators are collected simultaneously, with discrete vial samples collected periodically throughout data collection. We also present a mathematical algorithm integrating all data collected for the routine calibration of the GMC dataset. The algorithm facilitates comparison between the GMC and equilibrator datasets despite the substantial differences in response times (0.7-2.1 and 4.1-17.6 min, respectively). This measurement system was tested with both systematic laboratory experiments and field data collected on a research cruise along the US Atlantic margin. Once calibrated, this system identified numerous sharp peaks of dissolved methane concentration in the US Atlantic margin dataset that would be poorly resolved, or outright missed with previous measurement techniques. Overall, the precision and accuracy for the technique presented here were determined to be 11.2% and 10.4%, respectively, the operating range was 0-1000 ppm methane, and the e-folding response time to changes in dissolved methane concentration was 0.7–2.1 min.

Active sources and sinks of dissolved gases often lead to sharp spatial gradients in dissolved gas concentrations in marine and freshwater environments. Dissolved methane (CH<sub>4</sub>) concentrations span orders of magnitude in coastal and nearshore regions and the inability to accurately resolve these spatial gradients has led to large uncertainties in emissions

\*Correspondence: jdugan8@ur.rochester.edu

**Author Contribution Statement:** All authors designed the analytical system and correlation algorithm, and participated in field data collection. J.D and J.K conducted the laboratory experiments. J.D. wrote the initial manuscript, while all authors contributed to manuscript editing and revision. All authors give final approval for publication.

Additional Supporting Information may be found in the online version of this article.

estimates from these regions (e.g., Bastviken et al. 2004; Weber et al. 2019). Previous measurement techniques to quantify spatial dissolved concentration gradients have either relied on the collection of discrete samples or the use of continual underway measurements, both of which have limitations. Discrete sampling often lacks the sampling resolution necessary to characterize regional spatial gradients due to the necessary storage space and equipment for the collection and analysis of the samples (Wilson et al. 2018; Pohlman et al. 2021). Underway measurements are frequently hindered by long analytical response times, effectively averaging and smoothing spatial gradients (e.g., Gülzow et al. 2011), while also being prone to dilution from atmospheric contamination. These shortcomings limit the ability to quantify dissolved gas sources, sinks, and fluxes.

Most dissolved gas measurements are conducted in the gaseous phase rather than the aqueous phase. This requires that dissolved gases must either be equilibrated with a gaseous headspace or removed from the water entirely for analysis. This has been previously accomplished using discrete samples, equilibrators, or gas membrane contactors (GMCs; e.g., Johnson 1999; Gülzow et al. 2011; Magen et al. 2014; Hartmann et al. 2018; Joung et al. 2019). For discrete samples in vials, a headspace free of the desired gas is inserted and given sufficient time to reach equilibrium with the sample water. The partial pressure of the desired gas can then be measured in the headspace and related to the original dissolved concentration using the solubility of the gas and the headspace and water volumes (Upstill-Goddard et al. 1996; Magen et al. 2014). Discrete sampling often limits the spatial resolution of the study due to finite sample collection and storage capabilities, as well as relatively long total analysis times lasting minutes to hours per sample (e.g., Pohlman et al. 2021).

To improve the spatial resolution when mapping surface waters, equilibrators are commonly used to make continual underway measurements of dissolved concentrations (e.g., Gülzow et al. 2011; Grefe and Kaiser 2014). Equilibrators work by continuously flowing a sample water stream through an isolated headspace. This allows the dissolved gases in the water to reach equilibrium with the equilibrator headspace, which is continually analyzed (Johnson 1999). For low solubility gases, such as CH<sub>4</sub>, the slow equilibrator response times to changes in dissolved gas concentrations can lead to spatial imprecisions while measuring across gradients. However, for high solubility gases, such as carbon dioxide (CO<sub>2</sub>), the faster response times mitigate these imprecisions (e.g., Du et al. 2014; Pohlman et al. 2017). Equilibrators are also susceptible to venting of atmospheric gas into the headspace, pushing measured partial pressures away from that in the water stream and toward atmospheric values (Johnson 1999).

GMCs are also used to make continual dissolved gas concentration measurements and respond much faster than equilibrators to dissolved concentration changes (Hales et al. 2004; Hartmann et al. 2018). GMCs function by creating a partial pressure gradient across a gas permeable membrane that allows for gas exchange without the gaseous phase coming into contact with the liquid (Jiménez-Robles et al. 2021). Water flows through the inner shell of the GMC, inside the membrane. A partial pressure gradient is formed in the outer shell of the GMC by either creating a partial vacuum (Bandara et al. 2011), flowing a pure sweep gas along the membrane (McLeod et al. 2016), or a combination of both (Jiménez-Robles et al. 2021). All methods rarely extract 100% of the dissolved gas, and the extraction efficiency may change with environmental or membrane conditions (Sengupta et al. 1998; Jiménez-Robles et al. 2021; Velasco et al. 2022). In addition, the sweep gas dilutes the extracted gas. Thus, all GMC methods lead to raw measurements that require routine calibration to accurately represent the true environmental partial pressure of the dissolved gas.

Here we present an underway system to measure the dissolved concentration of CH<sub>4</sub> continually and accurately in surface water at high resolution, by combining the strengths of the three measurement methods outlined above. Water is pumped from the surface of the ocean aboard the ship and is split between a GMC and two Weiss-style equilibrators. Gas concentration data are collected simultaneously from the GMC and equilibrators, with discrete water samples collected periodically in vials. A calibration process using an optimization algorithm was developed to enable the correlation of the datasets and provide the coefficients necessary for calibration of the GMC while underway. This enables the GMC to be routinely calibrated in the field, correcting for variations in instrument performance on approximately daily timescales due to changing environmental and experimental conductions, and ultimately producing high-accuracy and high-spatial resolution maps of dissolved CH<sub>4</sub> concentrations in surface water.

#### Materials and procedures

In this section, we describe our instrumentation design for underway data collection combining GMC, equilibrator, and vial measurements. In addition, we present a mathematical calibration algorithm for the reconstruction of environmental  $\mathrm{CH_4}$  partial pressure, with spatial precision informed by the GMC and magnitude informed by equilibrator and discrete vial measurements.

# Underway data collection

To pump surface water aboard the ship, a submersible well pump (Dayton 1LZT3 Deep Well Submersible Pump, flow rate 20 GPM [75.71 L min $^{-1}$ ]) is secured in the surface mixed layer (Fig. 1). Water is pumped through suction hose (1 in [2.5 cm] inner diameter [ID]) aboard the ship. To remove solid material from the water stream and limit fouling of the GMC, water is flowed sequentially through 100-, 50-, and 10- $\mu$ m filters (Pentair Pentek 10-in. filter housing with polypropylene filter bags with plastic flange). The water stream is split between two Weiss-style equilibrators, a GMC (Liqui-Cel EXF series G453  $\times$ 50 membrane), and a water salinity and temperature sonde (YSI Model 600r multiparameter water quality sonde). There is also an additional water valve and outlet used to collect discrete water samples (Fig. 1).

The water directed to the equilibrators is split into two streams, a primary and secondary equilibrator. Water flow to each equilibrator is held constant at an average flow rate of  $2 \, \mathrm{L} \, \mathrm{min}^{-1}$  to each using a manual flow valve and water flow meter (WFM; Aalborg PWMS-010023) to the equilibrators. The water showers through the headspace of the equilibrators to maximize the water surface area and thus minimize equilibration time between the headspace and sample water stream. After flowing through the equilibrators, the water is returned

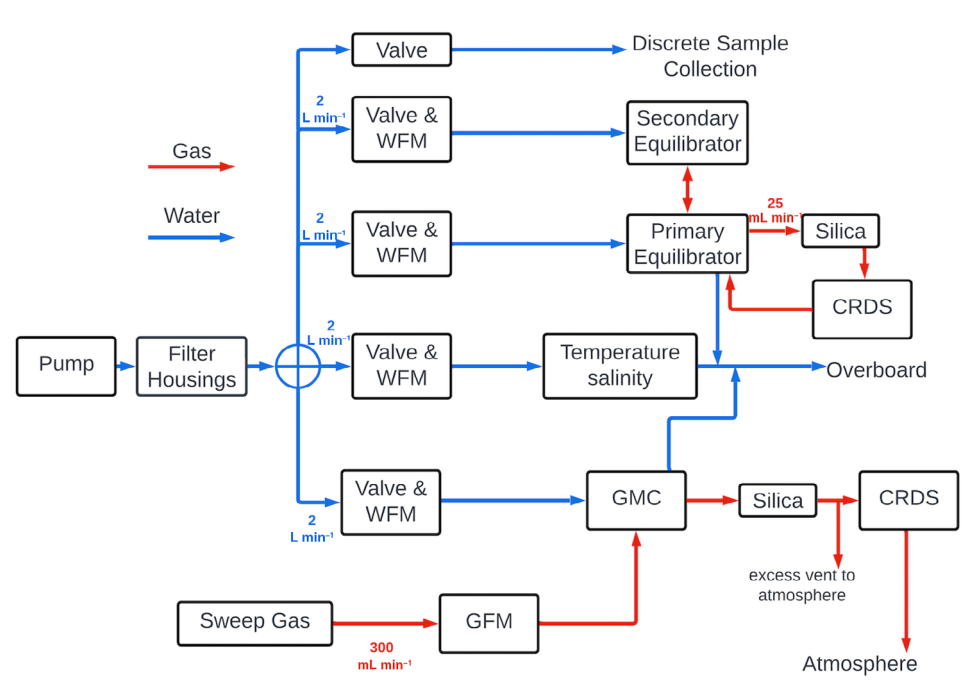


**Fig. 1.** Schematic of underway measurement system. A submersible pump is secured in the surface mixed layer. Water is pumped aboard the ship where it is filtered sequentially through 100-, 50-, and 10- $\mu$ m filters. The water is split between two equilibrators, a GMC, a water salinity and temperature sonde, and an outlet for discrete sample collection. Water flows to the equilibrators, GMC, and sonde at an average flow rate of 2 L min<sup>-1</sup> to each component controlled by a manual flow valve and measured by WFMs. A sweep gas of pure N<sub>2</sub> is flowed through the GMC controlled by a GFM at 300 mL min<sup>-1</sup>. The primary equilibrator and GMC are measured by CRDSs. Silica gel desiccation traps are used to dry the gas streams before analysis by the CRDSs.

overboard. To analyze the CH<sub>4</sub> partial pressure, the primary equilibrator headspace is continuously pumped to a cavity ringdown spectrometer (CRDS; Picarro G2201-i, flow rate 25 mL min<sup>-1</sup>) through  $\sim 15$  m of PVC plastic tubing (1/16<sup>th</sup> inch [1.59 mm] ID) at a rate of 25 mL min<sup>-1</sup> by the internal pump of the CRDS. After analysis, the gas is returned through  $\sim 15$  m of PVC plastic tubing to the primary equilibrator, establishing a closed analytical loop. The length of tubing was chosen to allow the water management system to be housed in the wet lab of a research vessel and the spectrometers in the dry lab; however, this length can be changed for different experimental arrangements. It takes  $\sim$  3 min for the gas to complete this loop and be returned to the primary equilibrator headspace. The headspace gas is passed through a silica gel desiccation trap to prevent a high concentration of water vapor from entering the CRDS. To minimize the influence of venting of atmospheric air into the equilibrator-CRDS analytical loop, the headspace of the primary equilibrator is connected to the secondary equilibrator with plastic tubing (1/8<sup>th</sup> inch [3.18 mm] ID), and the secondary equilibrator is vented to the atmosphere. This allows the secondary equilibrator to serve as a reservoir of partially equilibrated gas from which the primary equilibrator can draw rather than directly pulling from the atmosphere.

The water directed to the GMC flows through a manual flow valve and WFM at an average flow rate of 2 L min<sup>-1</sup>, within the recommended flow rate guidelines for this GMC.

The water flows through the inner shell of the GMC and the degassed water is returned overboard. The vacuum gas extraction method was initially used to avoid the need for a cylinder of sweep gas during field work; however, the bulk pressure gradient formed using this method caused water to leak through the membrane into the outer shell causing additional complications for analytical measurement. To avoid this problem, the sweep gas method was used to form the partial pressure gradient, without the same bulk pressure gradient. The flow rate of the sweep gas (nitrogen, N2) is held constant at 300 mL min<sup>-1</sup> using a gas flow meter (GFM; Aalborg, GFC 17). The gas flows through the outer shell of the GMC and a silica gel desiccation trap before being directed to the CRDS inlet (Picarro G2401, flow rate 275 mL min<sup>-1</sup>). The gas stream is held at a higher flow rate than the internal pump of the CRDS, with the excess vented to the atmosphere at the inlet of the CRDS thus preventing unnecessary pressurization of the CRDS analytical cavity.

The spectrometers used here were incorporated due to their availability in the investigators' laboratory. The Picarro G2201-i CRDS measures CH<sub>4</sub>, CO<sub>2</sub>,  $\delta^{13}$ C-CH<sub>4</sub>, and  $\delta^{13}$ C-CO<sub>2</sub> with measurement intervals at approximately 5 s and an inlet gas flow rate of approximately 25 mL min<sup>-1</sup>. The Picarro G2401 CRDS measures CH<sub>4</sub>, CO<sub>2</sub>, and carbon monoxide with measurement intervals at an average of 2.5 s and an inlet gas flow rate of approximately 275 mL min<sup>-1</sup>. Other field deployable spectrometers may be used, provided they have the

accuracy, precision, sensitivity, and measurement rate for the environmental gradients to be investigated.

Discrete samples were collected in 300-mL glass vials following a procedure similar to Magen et al. (2014) and Leonte et al. (2017). Vials were filled using plastic tubing connected to a manual flow valve, to allow for water flow rate control. The tubing was inserted to the bottom of the glass vials for appropriate vial flushing and filling. Vials were flushed with greater than three vial volumes and filled. The tubing was slowly removed while the flow rate was reduced to minimize agitation of the water surface. The vials were immediately capped with butyl rubber stoppers and sealed with aluminum crimp caps, after which a gaseous headspace of 10 mL of N<sub>2</sub> was inserted via displacement. To halt further biological activity, 0.5 mL of 8 mol L<sup>-1</sup> potassium hydroxide solution was injected, and the vials were stored at 5°C for 24 h to allow the N<sub>2</sub> headspace and sample water to reach equilibrium with respect to dissolved CH<sub>4</sub> partial pressure (pCH<sub>4</sub>). After 24 h, the headspace was removed and analyzed via gas chromatography with a flame ionization detector (Agilent 6850). Since the discrete vial samples contribute to the calibration of the GMC, we recommend the collection of vial samples at regular intervals throughout data collection, as well as when significant concentration gradients are observed.

#### Calibration method

The use of a sweep gas in a GMC alters the determination of pCH<sub>4</sub> because it both dilutes the extracted gas, and the extraction efficiency is likely not 100%. Therefore, underway GMC measurements can resolve spatial gradients in pCH<sub>4</sub>, but do not accurately capture the magnitude of pCH<sub>4</sub>, requiring routine calibration. The equilibrator data series and discrete vial measurements provide complementary datasets for GMC calibration because they can more accurately capture the magnitude of pCH<sub>4</sub>, despite being unable to precisely measure the spatial structure of gradients. However, discrete measurements and equilibrator data are subject to their own limitations for use in calibration. Discrete measurements often cannot be collected with sufficient frequency for robust calibration, whereas equilibrators are limited by their response time and are susceptible to venting of atmospheric air altering the measurement of pCH<sub>4</sub>. We therefore developed an algorithm that uses both continual equilibrator data series and periodic discrete measurements to calibrate the GMC data series. The method rests on a mechanistic understanding of how the pCH<sub>4</sub> determined by the GMC ( $P_{GMC}$ ) relates to that measured by the equilibrator  $(P_{eq})$ , while incorporating periodic discrete measurements of pCH<sub>4</sub> (P<sub>disc</sub>) to correct for commonplace venting in the equilibrator-CRDS analytical loop (Johnson 1999). The calibration process is described mathematically below and is illustrated in Fig. 2.

This calibration method assumes that although  $P_{\rm GMC}$  does not respond instantly to changes in dissolved pCH<sub>4</sub>, its

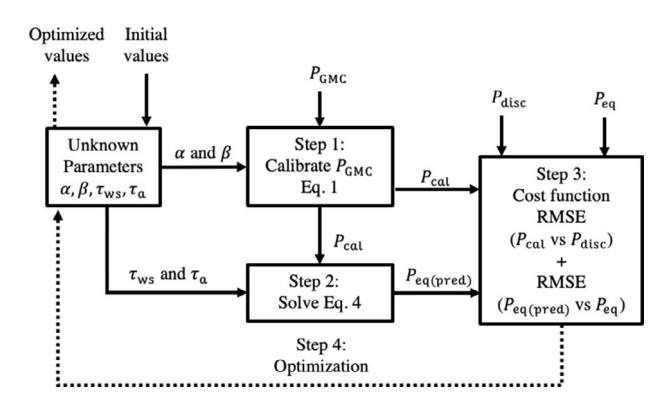


**Fig. 2.** Schematic diagram showing the optimization calibration process. The algorithm facilitates comparison of the GMC data series ( $P_{\rm GMC}$ ), the equilibrator data series ( $P_{\rm eq}$ ), and the discrete vial data ( $P_{\rm disc}$ ) using a genetic optimization algorithm to find the values for the slope ( $\alpha$ ),  $\gamma$ -intercept ( $\beta$ ), and response times of the equilibrator ( $\tau_{\rm ws}$  and  $\tau_{\rm a}$ ) which result in the best agreement between the three datasets.

response time ( $\tau_{\rm GMC}$ , i.e., the *e*-folding time) is fast enough to maintain a linear relationship between  $P_{\rm GMC}$  and the true environmental pCH<sub>4</sub> ( $P_{\rm env}$ ; Eq. 1).

$$P_{\rm env} \approx \alpha \times P_{\rm GMC} + \beta \equiv P_{\rm cal}$$
 (1)

Our goal is to find the optimum values of the calibration coefficients, slope ( $\alpha$ ) and y-intercept ( $\beta$ ), which bring the calibrated GMC data series ( $P_{cal}$ ) into the best agreement with two independent constraints on  $P_{\text{env}}$ . First,  $P_{\text{disc}}$  provides the most accurate instantaneous measurement of  $P_{env}$ , and therefore the optimum values of  $\alpha$  and  $\beta$  should minimize the difference between  $P_{\text{cal}}$  and  $P_{\text{disc}}$  at the time points where discrete measurements were collected. In the absence of other constraints,  $\alpha$  and  $\beta$  can be determined from linear correlation between  $P_{\rm GMC}$  and  $P_{\rm disc}$ , although this results in a large parameter uncertainty since vial measurements are often sparse (see "Assessment of uncertainty, accuracy, and precision" section). Second, a data series of  $P_{eq}$ , collected simultaneously with  $P_{\rm GMC}$ , provides an additional constraint on  $\alpha$  and  $\beta$  that is less direct, but more data rich. More specifically, the direct calibration of  $P_{GMC}$  with  $P_{eq}$  (i.e., by correlation) produces significant uncertainty due to differences in response times for the two techniques ( $\tau_{\rm eq}$  vs.  $\tau_{\rm GMC}$ ). However, when  $P_{\rm GMC}$  is mathematically smoothed in a similar manner to how the equilibrator mechanically smooths the environment, an equilibrator-based calibration can be conducted with minimal uncertainty.

The mathematical smoothing of  $P_{\rm GMC}$  is conducted as follows. First, an equation is established modeling the time (t) tendency of pCH<sub>4</sub> measured by the equilibrator (Eq. 2), which is equivalent to eq. 8 in Johnson (1999):

$$\frac{dP_{\text{eq}}}{dt} = \frac{1}{\tau_{\text{ws}}} \left( P_{\text{env}} - P_{\text{eq}} \right) + \frac{1}{\tau_{\text{a}}} \left( P_{\text{a}} - P_{\text{eq}} \right) \tag{2}$$

Here  $P_a$  is the pCH<sub>4</sub> of atmospheric air venting into the equilibrator-CRDS analytical loop. Equation 2 shows that  $P_{\rm eq}$  responds to changes in  $P_{\rm env}$  supplied through the sample water stream over a timescale ( $\tau_{\rm ws}$ ). In addition,  $P_{\rm eq}$  responds to venting atmospheric air into the equilibrator-CRDS analytical loop over a timescale ( $\tau_{\rm a}$ ). The observed total response time of the equilibrator ( $\tau_{\rm eq}$ ) is governed by both  $\tau_{\rm ws}$  and  $\tau_{\rm a}$  (Johnson 1999):

$$\frac{1}{\tau_{\rm eq}} = \frac{1}{\tau_{\rm WS}} + \frac{1}{\tau_{\rm a}} \tag{3}$$

Substituting  $P_{\rm cal}$  in Eq. 1 for  $P_{\rm env}$  in Eq. 2 produces Eq. 4. Solving Eq. 4 using Euler's method mathematical transforms the  $P_{GMC}$  data series by smoothing over the same timescales as the equilibrator, producing a prediction of  $P_{\rm eq}$  ( $P_{\rm eq(pred)}$ ):

$$\frac{dP_{\text{eq(pred)}}}{dt} = \frac{1}{\tau_{\text{ws}}} \left( \alpha * P_{GMC} + \beta - P_{\text{eq(pred)}} \right) + \frac{1}{\tau_{\text{a}}} \left( P_{\text{a}} - P_{\text{eq(pred)}} \right) \quad (4)$$

This smoothing process facilitates direct comparison between the GMC and equilibrator data series despite differences in  $\tau_{\rm eq}$  and  $\tau_{\rm GMC}$ , providing an additional constraint on  $\alpha$  and  $\beta$ . The optimum values of these parameters will lead to the closest agreement between  $P_{\rm eq}$  and  $P_{\rm eq(pred)}$ .

A confounding factor is that both equilibrator response times,  $\tau_{\rm ws}$  and  $\tau_{\rm a}$ , can vary considerably with environmental conditions and shipboard instrument configuration, meaning that they cannot be known a priori. Instead, this approach uses a four-step algorithm to find the optimum values for  $\alpha$ ,  $\beta$ ,  $\tau_{\rm ws}$ , and  $\tau_{\rm a}$  that produce the best correspondence between  $P_{\rm cal}$ ,  $P_{\rm eq}$ , and  $P_{\rm disc}$  (Fig. 2):

Step 1: A linear correlation is used between  $P_{\text{GMC}}$  and  $P_{\text{disc}}$  to produce initial estimates of  $\alpha$ ,  $\beta$ , and the  $P_{\text{cal}}$  data series.

Step 2: Eq. 4 is solved to form a  $P_{\text{eq(pred)}}$  data series.

Step 3: A cost function is evaluated that combines the root mean square errors (RMSE) between  $P_{\rm cal}$  and  $P_{\rm disc}$ , as well as between  $P_{\rm eq(pred)}$  and  $P_{\rm eq}$ , therefore weighting the two constraints outlined above equally.

Step 4: An optimization algorithm is used to iterate across the previous three steps, while adjusting the values of  $\alpha$ ,  $\beta$ ,  $\tau_{ws}$ , and  $\tau_a$  to minimize the cost function. For this step we use the genetic algorithm function from MATLAB's "Optimization Toolbox" (*see* Data availability statement for example codes).

Following this iterative process, the optimized values of  $\alpha$  and  $\beta$  are used to generate the final  $P_{\rm cal}$  data series. This can then be converted from pCH<sub>4</sub> to dissolved concentration using the salinity and temperature dependent solubility coefficients (Wiesenburg and Guinasso 1979).

We note that the calibration approach described above can be applied in the absence of discrete vial measurements, using  $P_{\rm eq}$  as the only constraint, in which case the cost function only includes the RMSE between  $P_{\rm eq(pred)}$  and  $P_{\rm eq}$ . However,

this results in a more uncertain calibration, because without discrete vials,  $\tau_a$  cannot be constrained as accurately (*see* "Assessment of uncertainty, accuracy, and precision" section).

For example codes, see Data availability statement.

#### Assessment

Systematic laboratory and field experiments were designed to test the functionality of the new technique and calibration method, and were used to quantify the accuracy, precision, operating range, and response time for the system described here. We emphasize that the operational parameters will change with (1) different extraction efficiencies of the GMC, associated with variations in environmental conditions, membrane age, purity, and type (Velasco et al. 2022), as well as (2) the incorporation of different spectrometers in the underway data collection system. We reiterate that these variations in operation parameters with changes in natural and experimental conditions are the very reason why this integrated calibration system was developed. Thus, the operational parameters presented here are an example of what is achievable with this technique.

#### Assessment of operating range

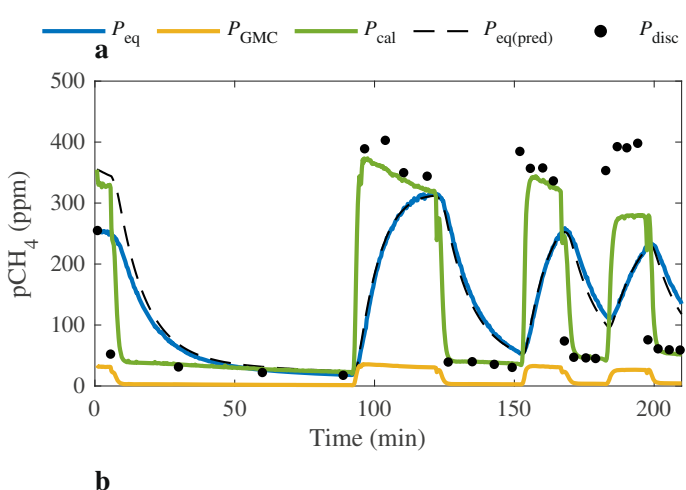
The operating range of the analytical system described here is dependent on the operating range of the specific spectrometers used. Although the GMC dilutes the dissolved pCH<sub>4</sub>, effectively expanding the operating range of the system, the equilibrator does not. And due to the need for continual equilibrator measurements for calibration, the operating range of the entire system is thus dependent on the operating range of the spectrometers incorporated. Care should be taken to ensure that the spectrometers employed have an operating range which brackets potential values of dissolved pCH<sub>4</sub> in the field.

# Assessment of response time $(\tau)$

A laboratory experiment was designed so that the response time of the equilibrators ( $\tau_{eq}$ ) could be independently determined using established methods and compared to those estimated by our calibration algorithm. This experiment also allowed for the independent verification of the GMC response time ( $\tau_{GMC}$ ).

Two 55-gallon barrels were used to house water whose dissolved pCH<sub>4</sub> were set to be different and varying with time. These water stores were used to represent environments with relatively low and high concentrations of dissolved CH<sub>4</sub> and were sequentially directed into the analytical system for response time assessment using a submersible well pump in each barrel (Supporting Information Fig. S1). As the pump transferred water, heat was generated noticeably increasing the water temperature in each barrel. Since this excess heat both changes the solubility of dissolved CH<sub>4</sub> and can cause the pump to shut off if its internal temperature reaches a

critical threshold, building water was flowed into the bottom of each barrel and out the top at an average rate of 3 L min<sup>-1</sup> for heat dissipation. This continuous flushing was effective at holding water temperature at  $\sim 25^{\circ}$ C. The pump in each barrel was connected to a three-way valve which could direct water back to its source barrel or through the analytical system. Water from one barrel was pumped through the analytical system at an average flow rate of 2 L min<sup>-1</sup> to each of the GMC, equilibrators, and water temperature and salinity sonde, controlled and measured by manual flow valves and WFMs. An additional outlet was used to collect discrete samples in 300-mL glass vials. Discrete samples were processed as described in the "Underway data collection" section following a procedure similar to Magen et al. (2014) and Leonte et al. (2017). For testing the GMC, a sweep gas (N2) was flowed through the outer shell at 300 mL min<sup>-1</sup>, controlled by a gas mass flow controller. The GMC gas stream was measured using a LI-COR LI-7180 CRDS. The primary equilibrator headspace



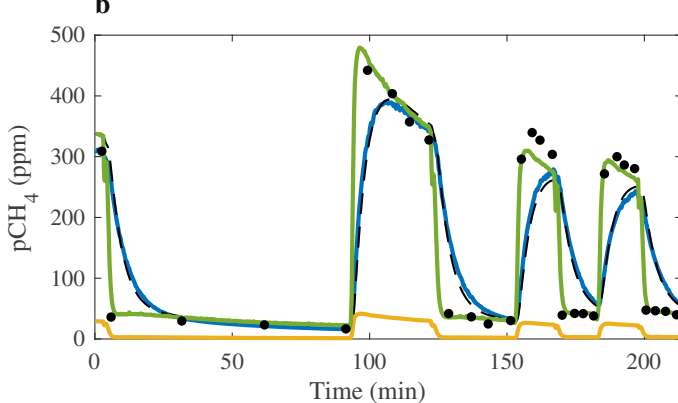


**Fig. 3.** Time series of laboratory data to test the system and calibration method. (**a**) pCH<sub>4</sub> as determined with the equilibrator ( $P_{eq}$ ), GMC ( $P_{GMC}$ ), calibrated GMC ( $P_{cal}$ ), predicted equilibrator ( $P_{eq(pred)}$ ), and discrete samples ( $P_{disc}$ ) for 175 mL min<sup>-1</sup> gas flow rate between the primary equilibrator headspace and CRDS. (**b**) Same as in (**a**) except for 275 mL min<sup>-1</sup> gas flow rate data series.

was analyzed using a Picarro G2401 CRDS and connected using  $\sim 15$  m of PVC plastic tubing. This CRDS was used to measure the primary equilibrator headspace instead of the Picarro G2201-i because it has a faster base flow rate, allowing for the flow rate to be adjusted over a wider range. Measurements were repeated with two gas flow rates between the primary equilibrator and CRDS, 175 and 275 mL min<sup>-1</sup>, in order to test the effectiveness of the calibration technique under different values of  $\tau_{eq}$  (Fig. 3). The flow rate between the primary equilibrator and CRDS effects  $au_{eq}$  because of the time it takes for gas to complete the equilibrator-CRDS analytical loop and establish equilibrium with the equilibrator headspace. By reducing the gas flow rate through the equilibrator headspace, tubing, and CRDS, the time necessary to fully homogenize the headspace gas and reach equilibrium with the inflowing sample water stream will increase. Data from the equilibrator and GMC were collected simultaneously in this experiment.

The low CH<sub>4</sub> concentration barrel was open to the atmosphere and had starting dissolved partial pressures of 18 and 16 ppm of CH<sub>4</sub> for the 175 and 275 mL min<sup>-1</sup> experiments, respectively according to the equilibrator. These pCH<sub>4</sub> are above ambient (ca. 2 ppm) and display background CH<sub>4</sub> in the building water used to continuously flush the barrels. The high CH<sub>4</sub> concentration water barrel was partially sealed and had N2 and CH4 added to increase the dissolved pCH4 while maintaining atmospheric pressure. The high CH<sub>4</sub> concentration barrel had starting dissolved pCH<sub>4</sub> of 252 ppm and 308 ppm of CH<sub>4</sub> for the 175 and 275 mL min<sup>-1</sup> experiments, respectively. The varying concentration of CH<sub>4</sub> in the building water, along with removal of CH<sub>4</sub> by the GMC, caused variations in dissolved pCH<sub>4</sub> in each barrel through the experiment; this had the welcome consequence of enabling technique assessment over a continuum of CH4 concentrations, while mimicking what is experienced in the natural environment. To simulate surveying across different water masses in the natural environment with different dissolved CH<sub>4</sub> concentrations, water flow to the analytical system was switched between high and low concentration barrels after  $\sim$  90, 30, 30, 15, 15, and 15 min. Discrete samples were collected immediately prior to each switch and three discrete samples were collected in the interim between switches for a total of 29 discrete samples per experiment.

The  $\tau_{\rm eq}$  and  $\tau_{\rm GMC}$  of the data series were calculated empirically using Eq. 5, which is an analytical solution describing how measured pCH<sub>4</sub> ( $P_{\rm meas}$ ) responds to changes in the environment (Garcia-Tigreros Kodovska et al. 2016):

$$\ln(P_{\text{meas}} - P_{\text{equilibrium}}) = \ln(P_{\text{meas}(i)} - P_{\text{equilibrium}}) - t \times \frac{1}{\tau}$$
 (5)

Here  $P_{\text{equilibrium}}$  is the measured pCH<sub>4</sub> when equilibrium was reached and  $P_{\text{meas}(i)}$  is the measured pCH<sub>4</sub> immediately before the sample water stream was switched to be sourced

**Table 1.**  $\tau$  values calculated empirically and using the calibration algorithm for  $P_{\text{eq}}$  and  $P_{\text{GMC}}$ .

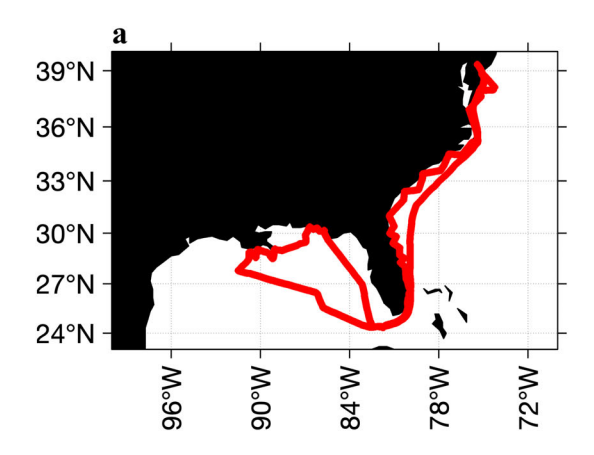
		$ au_{GMC}$ (min)			
		Empirical		Empirical	
Flow rate (mL min <sup>-1</sup> )	Calibration algorithm	Increasing	Decreasing	Increasing	Decreasing
175	10.13	9.08	25.77		
275	5.21	4.11	17.58		
N/A				0.70	2.10

from the other barrel. For each instrument,  $\tau$  was calculated as the inverse of the slope of  $ln(P_{meas} - P_{equilibrium})$  vs. t (Table 1). When the gas flow rate was  $175 \,\mathrm{mL\,min}^{-1}$ ,  $\tau_{\mathrm{eq}}$  was 9.08 and 25.77 min for increasing and decreasing concentrations of pCH<sub>4</sub>, respectively. When the gas flow rate was  $275 \,\mathrm{mL\,min}^{-1}$ ,  $\tau_{eq}$  was 4.11 and 17.58 min for increasing and decreasing concentrations of pCH<sub>4</sub>, respectively. Differences in  $\tau_{eq}$  between increasing and decreasing concentration periods is consistent with previous findings (Garcia-Tigreros Kodovska et al. 2016; Webb et al. 2016). The 275 mL min<sup>-1</sup> data series has a faster  $\tau_{eq}$  than the 175 mL min<sup>-1</sup> data series because of the shorter time it takes for the gas to travel through the equilibrator-CRDS closed analytical loop. Faster gas flow rates enable the gas in the equilibrator headspace, tubing, and CRDS to become fully homogenized and reach equilibrium with the inflowing sample water stream faster. The  $\tau_{GMC}$  was much faster than both the equilibrator data series, measuring 0.70 and 2.10 min when pCH<sub>4</sub> was increasing and decreasing, respectively. Since the response time is uninfluenced by the calibration procedure, the  $\tau_{GMC}$  determined here is the final response time of the system.

A detailed assessment of our calibration algorithm and its uncertainties is reserved for the next section using both laboratory and coastal ocean data. Here we simply assess its effectiveness at diagnosing  $\tau_{\rm eq}$ . When applied to the 175 mL min $^{-1}$  (Fig. 3a) and 275 mL min $^{-1}$  experiments (Fig. 3b), the mathematical smoothing operation (i.e., solution to Eq. 4) successfully transformed the  $P_{\rm GMC}$  data series into a  $P_{\rm eq(pred)}$  data series that closely resembled the real  $P_{\rm eq}$  measurements ( $R^2 = 0.95$  and 0.99 for the 175 and 275 mL min $^{-1}$  experiments, respectively). To achieve this, the optimization algorithm selected  $\tau_{\rm eq}$  of 10.13 and 5.21 min for the 175 and 275 mL min $^{-1}$  experiments, respectively. Both these values are within the range of  $\tau_{\rm eq}$  determined empirically (Table 1), building confidence in this aspect of the calibration procedure.

# Assessment of uncertainty, accuracy, and precision

Here we present estimates of the accuracy and precision for the analytical technique and calibration method using data collected in the laboratory-based experiment described above (275 mL min<sup>-1</sup> experiment) and data collected in the field. It should be noted that these values reflect the performance possible using the specific data collection method and calibration technique presented here, but these operational parameters are subject to change with changes in experimental conditions



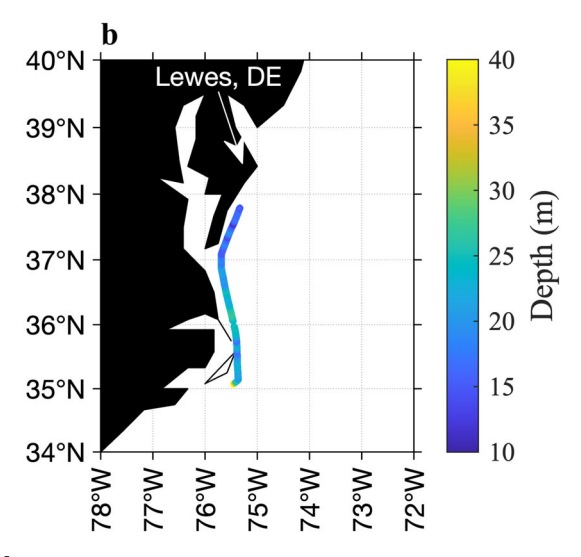


**Fig. 4.** Maps showing cruise tracks for the 2022 research cruise on the R/V *Hugh R. Sharp* along the US Atlantic margin and Gulf of Mexico. (a) Full cruise tracks. The research cruise left out of Lewes, Delaware moving southward rounding the Florida peninsula through the Gulf of Mexico and returned to Lewes, Delaware. (b) Cruise tracks for the subset of the field data used in the testing of uncertainty in the calibration method.

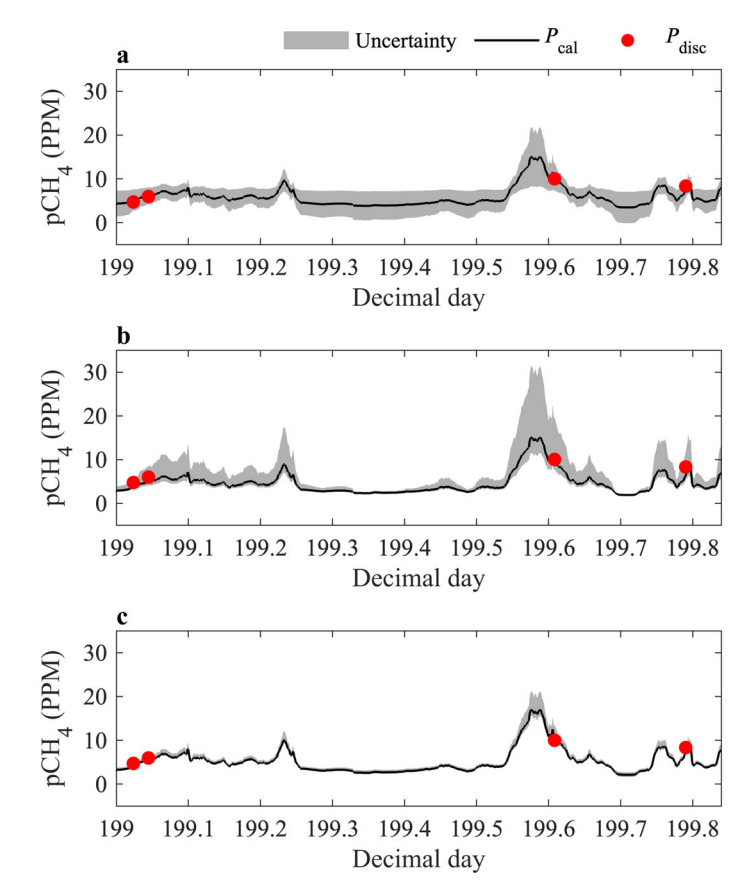


**Fig. 5.** Calibration of data series ( $P_{\rm cal}$ ) using only the (**a**) discrete measurements ( $P_{\rm disc}$ ), (**b**) equilibrator data series ( $P_{\rm eq}$ ), and (**c**) and the full calibration method using both  $P_{\rm disc}$  and  $P_{\rm eq}$  data series for the field data collected on 18 July 2022 along the US Atlantic margin. In (**b**) and (**c**), the black line represents calibration using 100% of available data, while uncertainty ranges are estimated with a bootstrapping approach.

(e.g., equilibrator-CRDS gas flow rate, GMC membrane age and purity,  $\mathrm{CH_4}$  analytical spectrometers). However, these effects caused by changes in environmental and operational conditions are the specific reason this underway calibration method was developed.

From 24 June 2022 to 19 July 2022, this analytical system was tested on a research cruise aboard the R/V Hugh R Sharp along the US Atlantic margin and Gulf of Mexico (Fig. 4a). The system was installed as described in the "Underway data collection" section. To prevent clogging and water vapor saturation, the water filters and silica gel in the desiccation traps were changed daily or as needed. A subset of the cruise dataset collected on 18 July 2022 (day-of-year 199-199.84; Fig. 4b) is used here as part of our assessment of the performance of the calibration method under oceanographic conditions while data from the entire expedition were used to assess accuracy and precision (Fig. 5). The portion of the cruise on 18 July 2022 occurred along the Atlantic margin of Maryland and Delaware traveling northbound, where water column depth ranged from 11.24 to 48.24 m. This portion of the dataset was chosen as it displayed several peaks of various sizes as well as periods of relatively stable pCH<sub>4</sub> in the  $P_{eq}$  data series, with values ranging from 2.11 to 10.49 ppm CH<sub>4</sub>.

To test the calibration algorithm and assess how the discrete measurement and equilibrator data influence uncertainty in the calibration parameters, the calibration process was tested using three sets of reference data for both the field- and laboratory-based data: (1) only  $P_{\rm disc}$ , (2) only  $P_{\rm eq}$ , and (3) the full calibration using both data sets (Table 2; Fig. 5; Supporting Information Fig. S2). To calibrate the  $P_{\rm GMC}$  data series using only  $P_{\rm disc}$ , the linear relationship between the two datasets was used as in Eq. 1, and the correlation coefficients  $\alpha$  and  $\beta$  of this relationship were applied to the full  $P_{\rm GMC}$  data series (Fig. 5a; Supporting Information Fig. S2a). The uncertainty in this calibration was quantified using the 95% confidence bounds from the linear least squares relationship (Table 2).

To calibrate using only the  $P_{\rm eq}$  data series,  $\alpha$ ,  $\beta$ ,  $\tau_{\rm ws}$ , and  $\tau_{\rm a}$  were optimized to minimize the RMSE between  $P_{\rm eq(pred)}$  and  $P_{\rm eq}$  (Fig. 2; Table 2), and the optimized  $\alpha$  and  $\beta$  were applied to  $P_{\rm GMC}$  data series (Fig. 5b; Supporting Information Fig. S2b). The uncertainty of  $\alpha$ ,  $\beta$ ,  $\tau_{\rm ws}$ , and  $\tau_{\rm a}$  were estimated with a bootstrapping approach, in which the process was repeated 1000 times, using 50% of the data each time. We report the 2.5–

**Table 2.**  $\alpha$ ,  $\beta$ ,  $\tau_{ws}$ , and  $\tau_a$  for calibration of  $P_{GMC}$  using only  $P_{disc}$ , only  $P_{eq}$ , and the full calibration using both  $P_{disc}$  and  $P_{eq}$  for the field data collected on 18 July 2022, and the 275 mL min<sup>-1</sup> gas flow rate experiment. Values inside parentheses are 95% uncertainty bounds. In the equilibrator-only calibration, we note that while the two equilibration timescales,  $\tau_{ws}$  and  $\tau_a$ , are individually uncertain, the overall response time,  $\tau_{eq}$  (Eq. 3), is very well constrained by the temporal relationship between  $P_{eq}$  and  $P_{GMC}$  and is between 19 and 20 min for the field data and 4–6 min in the laboratory data in all 1000 bootstrapping iterations.

Experiment	Calibration method	α	β	$ au_{ws}$ (min)	τ <sub>a</sub> (min)
Field	Discrete only	7.38 (1.18, 13.57)	1.52 (-3.59, 6.62)		
	Equilibrator only	7.16 (6.13, 15.80)	-0.0064 (-2.50, 0.26)	23.04 (19.73, 50.40)	12.57 (10.51, 60.048)
	Full calibration	9.50 (8.53, 12.37)	-0.41 (-1.63, 0.28)	30.24 (27.36, 40.32)	48.96 (37.44, 56.16)
Laboratory	Discrete only	11.51 (10.97, 12.05)	3.27 (-7.04, 13.58)		
	Equilibrator only	11.20 (10.97, 11.68)	9.81 (7.52, 10.28)	5.21 (5.00, 73.96)	175.54 (5.60, 1439.9)
	Full calibration	11.33 (11.06, 11.73)	7.86 (6.00, 9.43)	5.09 (5.00, 5.84)	164.93 (83.58, 1492.0)

97.5 percentile range (i.e., 95% confidence bounds) in parameter values (Table 2) and  $P_{\text{cal}}$  (Fig. 5b; Supporting Information Fig. S2b), which are highly asymmetrical around the optimum values. Using 100% of the equilibrator data, our algorithm yields a relatively low  $P_{cal}$  data series that underpredicts the discrete vial measurements for the equilibrator-only calibration for the field data, whereas some of the bootstrapping iterations find much larger calibration slopes ( $\alpha$ ), resulting in  $P_{\text{cal}}$ that overpredicts the discrete data (Fig. 5b). This highlights the drawback of calibrating with equilibrators alone: an equilibrator can produce a very similar  $P_{eq}$  data series when (i) equilibrating with low environmental pCH<sub>4</sub> while slowly venting to the atmosphere (low  $\alpha$ , high  $\tau_a$ ) or (ii) equilibrating with high environmental pCH<sub>4</sub> while venting quickly with the atmosphere (high  $\alpha$ , low  $\tau_a$ ). Therefore, due to uncertainty in equilibrator venting, the calibration parameters remain poorly constrained for the equilibrator-only calibration (Table 2).

The full calibration was completed using both  $P_{\text{disc}}$  and  $P_{\text{eq}}$ as described in "Calibration method" section (Fig. 5c; Supporting Information Fig. S2c) and uncertainty in  $\alpha$ ,  $\beta$ ,  $\tau_{ws}$ , and  $\tau_a$  were determined using the same bootstrapping process outlined in the paragraph above (Table 2). This resulted in much smaller uncertainty ranges in  $P_{cal}$  than the other two calibration approaches for both the field and laboratory data. Compared to the calibration with  $P_{\text{disc}}$  alone, the inclusion of equilibrator data compensates for data paucity and narrows the viable range of  $\alpha$  and  $\beta$ . Compared to calibration with only  $P_{\rm eq}$  for the field data, the incorporation of vial data excludes both scenarios with high  $P_{\rm env}$  and low  $\tau_a$  and scenarios with low  $P_{\rm env}$  and high  $\tau_a$ . Instead, the optimized parameters suggest our equilibrator was inadvertently venting at a moderate rate  $(\tau_a = 49 \text{ min})$  that is slower than the equilibration time with the water stream ( $\tau_{ws} = 30 \text{ min}$ ), but still fast enough that the equilibrator systematically underestimates  $P_{\rm env}$  (Fig. 6). It should be noted that during field data collection, the CRDS used to measure the equilibrator headspace pCH<sub>4</sub> has a gas flow rate of  $\sim 25 \, \text{mL} \, \text{min}^{-1}$  resulting in the slow equilibrator response times. For the laboratory data, the CRDS used to

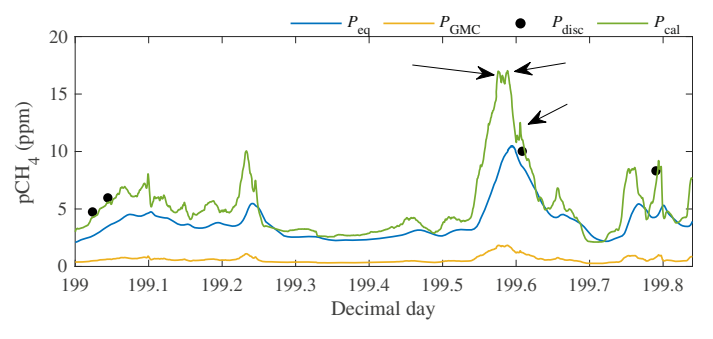


**Fig. 6.** Equilibrator ( $P_{eq}$ ), GMC ( $P_{GMC}$ ), discrete ( $P_{disc}$ ), and calibrated ( $P_{cal}$ ) data from the research cruise collected on 18 July 2022 (day-of-year 199–199.84). Arrows show three small pCH<sub>4</sub> subpeaks that are apparent in the  $P_{cal}$  data series, but not  $P_{eq}$  data series.

**Table 3.** Accuracy and precision of the system calculated using the field and laboratory data. The field data are from the 2022 research cruise along the US Atlantic margin and Gulf of Mexico and covers four days and includes 16 discrete measurements. The laboratory data are from the 275 mL min<sup>-1</sup> gas flow rate experiment and includes 29 discrete measurements.

		MAPE (accuracy) (%)	RMSPE (precision) (%)
Field	$P_{\rm cal}$	10.4	11.2
	$P_{\rm eq}$	108.8	47.2
Laboratory	$P_{\rm cal}$	15.0	27.9
	$P_{\rm eq}$	100.7	178.8

measure the equilibrator headspace pCH<sub>4</sub> had a must faster flow rate and the optimized parameters suggest that the equilibrator was venting very slowly ( $\tau_a = 165 \, \text{min}$ ), with an equilibration time ( $\tau_{ws} = 5 \, \text{min}$ ; Table 2) that is in line with the  $\tau_{eq}$  values that was calculated empirically (Table 1). These results show that if there was an equilibrator leak in the laboratory experiment, it was very slow. Together, our field and laboratory assessments underscore the calibration method's ability to diagnose accurate values of  $\alpha$  and  $\beta$  regardless of the equilibrator leak magnitude, by jointly leveraging the equilibrator and discrete vial measurements as constraints.

The accuracy and precision of the final  $P_{\text{cal}}$  data series (Fig. 5c; Supporting Information Fig. S2c) were assessed through comparison with  $P_{\text{disc}}$  (Table 3). For the field data, the full calibration process was completed for four days of the research cruise and included a total of 16 discrete measurements. For the laboratory data, the full calibration was applied to the 275 mL min<sup>-1</sup> experiment data and included a total of 29 discrete measurements. The accuracy and precision of  $P_{eq}$  is included as a comparison to a commonly used technique for the underway measurement of pCH<sub>4</sub> in surface water. The accuracy between true  $P_{\text{env}}$  (in this case  $P_{\text{disc}}$ ) and  $P_{\text{cal}}$  or  $P_{\text{eq}}$ was assessed using the mean absolute percent error (MAPE). For the field data, the MAPE of  $P_{\text{cal}}$  was 10.36%, whereas the MAPE of  $P_{eq}$  was 108.83%. For the laboratory data, the MAPE of  $P_{\text{cal}}$  was 15.01%, whereas the MAPE of  $P_{\text{eq}}$  was 100.71%. The precision was assessed through the root mean square percent error (RMSPE) between  $P_{cal}$  or  $P_{eq}$  and  $P_{disc}$ . For the field data, the RMSPE of  $P_{\rm cal}$  was 11.23%, whereas the RMSPE of  $P_{\rm eq}$ was 47.21%. For the laboratory data, the RMSPE of  $P_{\text{cal}}$  was 27.93%, whereas the RMSPE of  $P_{eq}$  was 178.82%. The  $P_{cal}$  data series was therefore significantly more accurate and precise than using an equilibrator alone.

#### Discussion

# Proof of concept

The 18 July 2022 research cruise data subset is used here to highlight the advantages of this new analytical system and

calibration method. A brief description of the data collection and environmental conditions is given in "Assessment of uncertainty, accuracy, and precision." Our method was able to collect data at a temporal resolution of  $\sim 7$  s, far beyond what would be possible using only discrete vial collection. In addition, the intercomparison of  $P_{eq}$  against  $P_{cal}$  highlights that new information was gained with this new measurement technique. For example, the measured peak values of pCH4 determined from  $P_{cal}$  were higher than those measured in the  $P_{eq}$ data series (Fig. 6). The largest peak in the data subset is between day of year 199.5 and 199.7, reaching an apex of 17.22 ppm  $CH_4$  in the  $P_{cal}$  data series, while only reaching  $10.49 \,\mathrm{ppm}$  CH<sub>4</sub> in the  $P_{\mathrm{eq}}$  series. The long analytical response time of the equilibrators elongates and dampens the measured pCH<sub>4</sub> peak. There is also a difference in the time when the apex of the peak was measured. The apex occurred at dayof-year 199.5883 in the  $P_{\text{cal}}$  data series and 199.5945 in the  $P_{\rm eq}$  data series. This corresponds to a difference of 8.93 min or 1.13 km. Precisely capturing the location and magnitude of surface water concentrations is important for accurately characterizing spatial gradients and attributing sources and sinks, which cannot be done using slow response equilibrators alone.

It is also possible to observe peaks in the  $P_{\rm cal}$  data series that were not captured in the  $P_{\rm eq}$  data series. This can be seen in the same peak between day-of-year 199.5 and 199.7 (Fig. 6). For example, near the top of the peak, the  $P_{\rm cal}$  data series records three subpeaks, while the  $P_{\rm eq}$  data series records one rounded peak. Overall, during this single day of measurement, eight additional peaks were observed in the  $P_{\rm cal}$  data series, where a peak is defined as a peak-to-background change greater than 1 ppm CH<sub>4</sub>, that were invisible in the  $P_{\rm eq}$  data series.

## Comments and recommendations

Due to the relatively slow response time of low solubility gases like CH<sub>4</sub>, equilibrators are not able to fully resolve spatial changes in dissolved concentrations in coastal environments where relatively steep concentration gradients exist. Additionally, it is not feasible to collect discrete measurements at spatial resolutions high enough to resolve steep gradients over large geographic areas. GMCs are able to precisely measure dissolved concentration gradients, but require routine calibration to accurately represent the magnitude of dissolved concentrations. We have developed a system for the continual underway measurement and field-based calibration of dissolved CH<sub>4</sub> concentration in surface water. The system uses two water equilibrators and a GMC to collect continual data simultaneously, supplemented by periodic discrete measurements. This produces a final data series that retains the spatial

structure of a GMC data series, with magnitudes informed by discrete measurements and an equilibrator data series.

The use of equilibrators and discrete measurements enables the field-based calibration of the GMC data. The results of our field and laboratory trials indicate that response times can vary with experimental conditions, underscoring the need for routine field-based calibration, as opposed to pre- or post-cruise laboratory-based calibration. Changes in response times appear to be caused by slight changes in experimental and environmental conditions, some of which were likely temperature, salinity, or slight variations in gas or water flow rates. Similarly, we noticed that a change in the bulk pressure gradient across the GMC membrane can change extraction efficiency, thus calibration should be conducted when water or sweep gas flow is stopped and restarted. We also note that while we did not observe large degradation in GMC performance across the approximately month-long research expedition presented here, a decrease in membrane efficiency with time has been observed elsewhere (Velasco et al. 2022). Thus, the full calibration routine should be completed routinely and each time data collection is stopped to account for unseen changes in experimental conditions. We further recommend that discrete vial samples be collected periodically at regularly spaced intervals during underway data collection as well as across significant concentration gradients. This will ensure that there is sufficient discrete data over a range of time intervals and dissolved concentrations to produce a well constrained  $P_{\text{cal}}$  data series.

This system was designed to specifically measure dissolved CH<sub>4</sub> concentrations. High solubility gases, such as CO<sub>2</sub> are known to have relatively fast  $\tau_{eq}$ , likely rendering the extra complexity of this GMC-based system unnecessary if only dissolved CO<sub>2</sub> concentration is of interest.

#### Data availability statement

Example codes are available at https://doi.org/10.5281/zenodo.10215090. Example data is available at https://doi.org/10.60593/ur.d25481641.

#### References

Bandara, W. M. K. R. T. W., H. Satoh, M. Sasakawa, Y. Nakahara, M. Takahashi, and S. Okabe. 2011. Removal of residual dissolved methane gas in an upflow anaerobic sludge blanket reactor treating low-strength wastewater at low temperature with degassing membrane. Water Res. **45**: 3533–3540. doi:10.1016/j.watres.2011.04.030

Bastviken, D., J. Cole, M. Pace, and L. Tranvik. 2004. Methane emissions from lakes: Dependence of lake characteristics, two regional assessments, and a global estimate. Global Biogeochem. Cycl. **18**: GB4009. doi:10.1029/2004GB002238

- Du, M., S. Yvon-Lewis, F. Garcia-Tigreros, D. L. Valentine, S. D. Mendes, and J. D. Kessler. 2014. High resolution measurements of methane and carbon dioxide in surface waters over a natural seep reveal dynamics of dissolved phase air– sea flux. Environ. Sci. Technol. 48: 10165–10173. doi:10. 1021/es5017813
- Garcia-Tigreros Kodovska, F., K. J. Sparrow, S. A. Yvon-Lewis, A. Paytan, N. T. Dimova, A. Lecher, and J. D. Kessler. 2016. Dissolved methane and carbon dioxide fluxes in Subarctic and Arctic regions: Assessing measurement techniques and spatial gradients. Earth Planet. Sci. Lett. **436**: 43–55. doi:10. 1016/j.epsl.2015.12.002
- Grefe, I., and J. Kaiser. 2014. Equilibrator-based measurements of dissolved nitrous oxide in the surface ocean using an integrated cavity output laser absorption spectrometer. Ocean Sci. **10**: 501–512. doi:10.5194/os-10-501-2014
- Gülzow, W., G. Rehder, B. Schneider, J. S. V. Deimling, and B. Sadkowiak. 2011. A new method for continuous measurement of methane and carbon dioxide in surface waters using off-axis integrated cavity output spectroscopy (ICOS): An example from the Baltic Sea. Limnol. Oceanogr. Methods 9: 176–184. doi:10.4319/lom.2011.9.176
- Hales, B., D. Chipman, and T. Takahashi. 2004. High-frequency measurement of partial pressure and total concentration of carbon dioxide in seawater using microporous hydrophobic membrane contactors. Limnol. Oceanogr. Methods **2**: 356–364. doi:10.4319/lom.2004.2.356
- Hartmann, J. F., and others. 2018. A fast and sensitive method for the continuous in situ determination of dissolved methane and its  $\delta^{13}$ C-isotope ratio in surface waters. Limnol. Oceanogr. Methods **16**: 273–285. doi:10.1002/lom3.10244
- Jiménez-Robles, R., C. Gabaldón, V. Martínez-Soria, and M. Izquierdo. 2021. Simultaneous application of vacuum and sweep gas in a polypropylene membrane contactor for the recovery of dissolved methane from water. J. Membr. Sci. **617**: 118560. doi:10.1016/j.memsci.2020.118560
- Johnson, J. E. 1999. Evaluation of a seawater equilibrator for shipboard analysis of dissolved oceanic trace gases. Anal. Chim. Acta **395**: 119–132. doi:10.1016/S0003-2670(99) 00361-X
- Joung, D., M. Leonte, and J. D. Kessler. 2019. Methane sources in the waters of Lake Michigan and Lake Superior as revealed by natural radiocarbon measurements. Geophys. Res. Lett. **46**: 5436–5444. doi:10.1029/2019GL082531
- Leonte, M., J. D. Kessler, M. Y. Kellermann, E. C. Arrington, D. L. Valentine, and S. P. Sylva. 2017. Rapid rates of aerobic methane oxidation at the feather edge of gas hydrate stability in the waters of Hudson Canyon, US Atlantic Margin. Geochim. Cosmochim. Acta **204**: 375–387. doi:10.1016/j. gca.2017.01.009
- Magen, C., L. L. Lapham, J. W. Pohlman, K. Marshall, S. Bosman, M. Casso, and J. P. Chanton. 2014. A simple

- headspace equilibration method for measuring dissolved methane. Limnol. Oceanogr. Methods **12**: 637–650. doi:10. 4319/lom.2014.12.637
- McLeod, A., B. Jefferson, and E. McAdam. 2016. Toward gasphase controlled mass transfer in micro-porous membrane contactors for recovery and concentration of dissolved methane in the gas phase. J. Membr. Sci. **510**: 466–471. doi:10.1016/j.memsci.2016.03.030
- Pohlman, J. W., J. Greinert, C. Ruppel, A. Silyakova, L. Vielstädte, M. Casso, J. Mienert, and S. Bünz. 2017. Enhanced CO<sub>2</sub> uptake at a shallow Arctic Ocean seep field overwhelms the positive warming potential of emitted methane. Proc. Natl. Acad. Sci. USA **114**: 5355–5360. doi: 10.1073/pnas.1618926114
- Pohlman, J. W., M. Casso, C. Magen, and E. Bergeron. 2021. Discrete sample introduction module for quantitative and isotopic analysis of methane and other gases by cavity ringdown spectroscopy. Environ. Sci. Technol. **55**: 12066–12074. doi:10.1021/acs.est.1c01386
- Sengupta, A., P. A. Peterson, B. D. Miller, J. Schneider, and C. W. Fulk Jr. 1998. Large-scale application of membrane contactors for gas transfer from or to ultrapure water. Sep. Purif. Technol. 14: 189–200. doi:10.1016/S1383-5866(98) 00074-4
- Upstill-Goddard, R. C., A. P. Rees, and N. J. P. Owens. 1996. Simultaneous high-precision measurements of methane and nitrous oxide in water and seawater by single phase equilibration gas chromatography. Deep-Sea Res. I Oceanogr. Res. Pap. **43**: 1669–1682. doi:10.1016/S0967-0637(96) 00074-X
- Velasco, P., V. Jegatheesan, and M. Othman. 2022. Effect of long-term operations on the performance of hollow fiber membrane contactor (HFMC) in recovering dissolved methane from anaerobic effluent. Sci. Total Environ. 841: 156601. doi:10.1016/j.scitotenv.2022.156601
- Webb, J. R., D. T. Maher, and I. R. Santos. 2016. Automated, in situ measurements of dissolved  $CO_2$ , CH4, and  $\delta^{13}C$  values using cavity enhanced laser absorption spectrometry: Comparing response times of air-water equilibrators. Limnol. Oceanogr. Methods **14**: 323–337. doi:10.1002/lom3.10092
- Weber, T., N. A. Wiseman, and A. Kock. 2019. Global ocean methane emissions dominated by shallow coastal waters. Nat. Commun. **10**: 4584. doi:10.1038/s41467-019-12541-7
- Wiesenburg, D. A., and N. L. Guinasso. 1979. Equilibrium solubilities of methane, carbon monoxide and hydrogren in water and sea water. J. Chem. Eng. Data **24**: 356–360. doi: 10.1021/je60083a006
- Wilson, S. T., and others. 2018. An intercomparison of oceanic methane and nitrous oxide measurements. Biogeosciences **15**: 5891–5907. doi:10.5194/bg-15-5891-2018

Mapping surface water CH<sub>4</sub> concentration

Submitted 03 May 2023 Revised 13 February 2024 Accepted 01 March 2024

Associate editor: Mike DeGrandpre

#### Acknowledgments

We are grateful to the captain and crew of the R/V Hugh R. Sharp who provided skillful assistance during research at sea. We are also grateful to Sydney Louden for her help conducting the laboratory research experiments. In addition, we are grateful to Madeline Every, Katherine Gregory, DongJoo Joung, and Rebecca Rust for assistance during field testing. This research was funded by grants to J.K. from National Science Foundation (NSF) (OCE-1634871 and OCE-2023514) and to J.K. and T.W. from the NSF (OCE-1851402).

## **Conflict of Interest**

None declared.